

Article

Dynamic Mechanical Behavior of Rock Specimens with Varying Joint Roughness and Inclination under Impact Load

Pu Yuan^{1,2,3} , Aobo Li^{1,*}, Changning Chen¹ and Qinghe Zhang^{1,2,3} 

¹ School of Civil Engineering and Architecture, Anhui University of Science and Technology, Huainan 232001, China; puy2012@126.com (P.Y.); ningchangchenaust@163.com (C.C.); zhangqhsdu@163.com (Q.Z.)

² State Key Laboratory of Mining Response and Disaster Prevention and Control in Deep Coal Mines, Anhui University of Science and Technology, Huainan 232001, China

³ Engineering Research Center of Underground Mine Construction, Ministry of Education, Anhui University of Science and Technology, Huainan 232001, China

* Correspondence: aob2023@126.com; Tel.: +86-157-3831-6393

Abstract: The influence of joint roughness and inclination on the dynamic mechanical properties of rocks is a prominent research area. In order to investigate the effects of joint roughness and inclination on the dynamic mechanical properties of jointed rocks, impact tests were conducted using a spilt Hopkinson pressure bar (SHPB) apparatus for prefabricated serrated joint cement mortar specimens with varying joint roughness and inclination. The failure mode, stress wave propagation characteristics, peak stress, and stress wave energy transfer law under impact load were analyzed. The results indicate that both joint inclinations and joint roughness coefficients (JRC) have a strong influence on the failure mode, peak stress, and stress wave energy transfer of jointed specimens. The jointed specimens exhibit three distinct failure modes under impact load, namely splitting tensile failure, shear slip failure, and compound failure of splitting tensile and shear. The peak stress initially decreases then increases with the increase in joint inclination angle, namely a V-shape variation, while it gradually increases with JRC increasing from 0 to 20. Jointed specimens exhibit the lowest peak stress at an inclination angle of 45° and JRC of 0. The variation of transmitted energy coefficient is similar to the peak stress, while the variation of reflected energy coefficient is opposite to the peak stress. At joint inclination angles of 0° or 90°, the reflected energy coefficient increases with the increase of JRC from 0 to 20, while the transmitted energy decreases. However, when the joint inclination angle is in the range of 30° to 60°, the reflected energy coefficient gradually decreases with JRC increasing, while the transmitted energy coefficient gradually increases.

Keywords: jointed rock mass; joint inclination; joint roughness; energy



Citation: Yuan, P.; Li, A.; Chen, C.; Zhang, Q. Dynamic Mechanical Behavior of Rock Specimens with Varying Joint Roughness and Inclination under Impact Load. *Appl. Sci.* **2023**, *13*, 8440. <https://doi.org/10.3390/app13148440>

Academic Editor: Arcady Dyskin

Received: 19 June 2023

Revised: 19 July 2023

Accepted: 20 July 2023

Published: 21 July 2023



Copyright: © 2023 by the authors. Licensee MDPI, Basel, Switzerland. This article is an open access article distributed under the terms and conditions of the Creative Commons Attribution (CC BY) license (<https://creativecommons.org/licenses/by/4.0/>).

1. Introduction

Joint is a prevalent geological structure that significantly influences the mechanical properties and engineering behavior of rocks [1,2]. Moreover, roughness and inclination are two critical parameters that govern the surface morphology of joints [3,4]. Joints play a significant role in the mechanical behavior of rocks, stress wave propagation, and failure process [5–7].

Previously, many scholars have researched the influence of jointed cracks in rock masses on dynamic mechanical properties [8–11] and damage mechanism [12–15]. The geometric parameters of the joints mainly include joint roughness, thickness, penetration, inclination, and opening degree [16,17]. Walton et al. [18] explored the impact of preset joints on key rock mass parameters, including stiffness, peak strength, and residual strength. Crampin [19] observed that the energy attenuation of stress waves passing through directionally arranged cracks exhibits a higher anisotropy than the wave velocity, which indicates that the energy attenuation is more sensitive to crack existence than wave velocity.

Hudson [20] revealed that the energy attenuation coefficient is proportional to the ratio of fracture density to the wavelength and the average fracture radius to the wavelength. Seinov and Chevkin [21] pointed out that the stress wave attenuation depends on the number and width of cracks and the wave impedance of the filler. Kahraman [22] simulated joint surface roughness by systematically depicting scratches on the rock surface, and further explored the relationship between stress wave velocity and joint surface roughness.

Liu et al. [23] investigated the effects of joint morphology, number of joints, loading strain rate, type, thickness of joint fillings, and specimen aspect ratio on the dynamic compressive strength and failure mode of jointed rock masses using a similar material model test. Li et al. [24–26] conducted SHPB tests for artificially formed jointed specimens with different joint roughness and analyzed the relationship between energy dissipation and fractal dimension of jointed specimens. Li et al. [27] investigated the impact of strain rate and penetration angle of joints on the failure mode, energy transfer, and dissipation law of simulated rock materials. Yang et al. [28] and Zhang et al. [29] researched the effect of joint thickness on the dynamic characteristics of rocks through similar material model experiments. Ping et al. [30] tested the dynamic compression mechanical properties of prefabricated fractured sandstone specimens with different angles and found that the fracture morphology at an inclination angle of 45° was the largest. Wang et al. [31,32] studied the effect of the through joint angle on the wave characteristics and energy dissipation of rock-like materials. In order to research the effect of joint rock parameters on rock failure, Zou et al. [33–35] explored the mechanical properties of jointed rocks using uniaxial compression tests by presetting joints with different angles in simulated materials. Tsubota et al. [36] conducted dynamic tests on natural rock joints using Ryoke gneiss to reveal the mechanical properties of natural joints and concluded that rock joint surface conditions such as roughness, hardness, and degree of weathering have significant effects on shear strength.

In the past research, scholars have paid extensive attention to the influence of jointed fractures in rock masses on the dynamic mechanical properties and failure mechanism. Nevertheless, there is a lack of in-depth research investigating the combined effects of joint roughness and inclination on the dynamic characteristics of jointed rocks. It has been pointed out that both joint roughness and inclination have a significant influence on the mechanical behavior of rocks, stress wave propagation, and specimen failure process. Moreover, the geometric parameters of joints, including roughness, thickness, penetration, inclination, and aperture, also significantly affect the mechanical properties of rocks. Although some studies have investigated the effects of certain parameters on rocks, the comprehensive investigation of the effects on the dynamic characteristics of jointed rock masses with varying joint roughness and inclination remains relatively limited.

In this study, impact tests were carried out by SHPB apparatus for prefabricated jointed cement mortar specimens with varying joint roughness and inclination. Subsequently, the dynamic mechanical properties, stress wave propagation characteristics, and failure behavior were evaluated based on the obtained results. The objective of this study is to explore the effect of joint roughness and inclination on the dynamic characteristics of rocks.

2. Materials and Methods

2.1. Joint Morphology Design

Due to the complexity of natural joints, artificially prefabricated jointed cement mortar specimens are adopted for serrated joint morphology studies. The serrated joint is simulated by the gypsum, and the rock is simulated by the cement mortar. In order to study the effect of joint roughness and inclination on dynamic mechanical properties and wave propagation characteristics, both joint roughness coefficient (JRC) and joint inclination angle were both varied for all through jointed specimens. Five joint roughness coefficients of 0, 5, 10, 15,

and 20 were designed, and five joint inclination angles of 0° , 30° , 45° , 60° , and 90° were considered. JRC was calculated with the fitting formula modified by Xie [37].

$$D = \log_{10} 4 / \log_{10} \left\{ 2 \left[1 + \cos \left(\tan^{-1} (2H/L) \right) \right] \right\} \quad (1)$$

$$\text{JRC} = 85.2671(D - 1)^{0.5679} \quad (2)$$

where D , L , and H represent the fractal dimension of joint, average base length, and average height of joint serration, respectively.

Schematic diagrams of the serrated joint with various JRCs are shown in Figure 1.

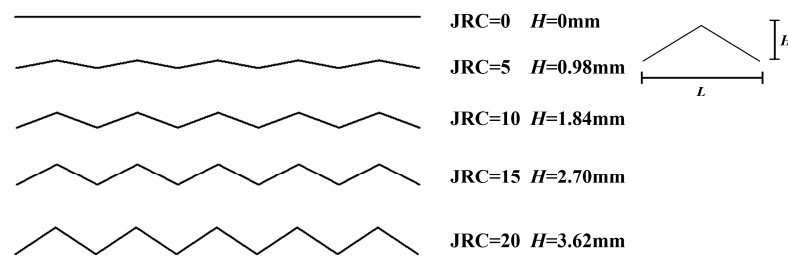


Figure 1. Schematic diagrams of serrated joints.

2.2. SHPB Apparatus

Impact tests were conducted using a variable cross-section SHPB apparatus, shown in Figure 2a. Both incident bar and transmission bar are steel bars with diameter of 50 mm and length of 2.4 m and 1.2 m, respectively. The incident bar has a 150 mm variable cross-section at the impact end, with the diameter ranging from 37 mm to 50 mm. The density and elastic modulus of steel bars are 7800 kg/m^3 and 210 GPa, respectively, and the longitudinal wave velocity is 5190 m/s. Stress wave signals are gathered by strain gauges attached to both incident bar and transmission bar. Data acquisition system comprised a dynamic strain indicator and an oscilloscope. During the impact tests, a jointed cement mortar specimen was sandwiched between the incident bar and the transmission bar to ensure coaxial alignment, as shown in Figure 2b. Vaseline was applied on the contact surfaces between jointed specimen and contact end of the compression bars to reduce frictional effect.

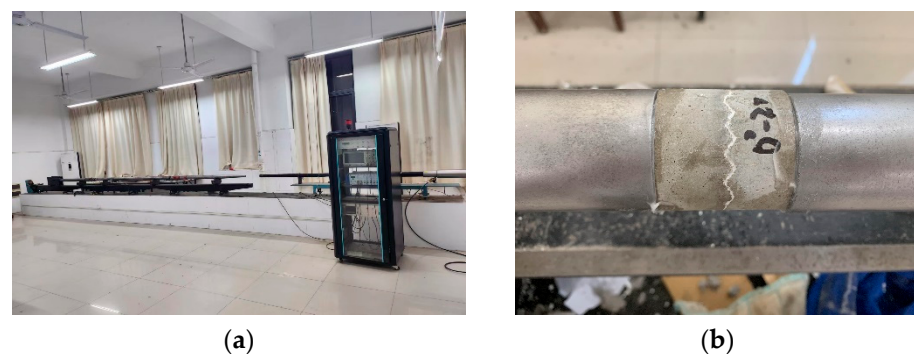


Figure 2. Schematic diagram of SHPB apparatus and specimen placement. (a) Variable cross-section SHPB apparatus, (b) Jointed specimen sandwiched between incident bar and transmission bar.

2.3. Jointed Specimen Preparation

Experimental investigation using natural rock materials have the following limitations. Firstly, as rock contains various minerals and internal defects, there is a certain dispersion of physical and mechanical parameters, which may lead to low consistency of repeated test results and cause errors. Secondly, it is difficult to process joints with various roughness on natural rock surface, and the natural rock may be damaged during the preparation process, resulting in test results not reflecting the effect of the joint roughness on the dynamic

mechanical properties. In contrast, cement mortar has physical and mechanical properties similar to rock materials, and it can be poured into any shapes, which can effectively solve the above problems.

Based on relevant literature [3,23,27] and orthogonal tests, five sets of mix proportion were designed, and a static uniaxial compression test has been conducted using an electro-hydraulic servo universal testing machine. In order to eliminate the discreteness of test results, three parallel tests have been carried out for each mix proportion of cement mortar. Ordinary Portland cement with 42.5 grade was adopted. Fine sand with maximum particle size of 0.6 mm was selected. According to the static test results, the mix proportion of the cement mortar was selected as cement:water:fine sand = 1:0.4:0.7. The corresponding physical and static mechanical parameters of cement mortar is shown in Table 1. In Table 1, f is static uniaxial compressive strength, ρ is density, E is elastic modulus, and μ is Poisson's ratio.

Table 1. Physical and static mechanical parameters of the cement mortar.

| Mix Proportion | f /MPa | ρ /(g·cm ⁻³) | E /GPa | μ |
|------------------------------------|----------|-------------------------------|----------|-------|
| cement:water:fine sand = 1:0.4:0.7 | 28.56 | 2.44 | 3.68 | 0.25 |

In order to prefabricate serrated joints in cement mortar specimens, 3D printing technology has been used to manufacture serrated joint surface molds with various JRCs and joint inclination angles.

The production process of jointed cement mortar specimen can be divided into five steps. Firstly, put the serrated joint surface mold into a standard cylindrical mold with lubricant oil on the inner wall, then brush the serrated joint surface with lubricant oil and compact moderately to prevent slippage during the vibration process. Secondly, weigh cement, water, and fine sand using an electronic scale according to the mix proportion, then put the cement and fine sand into a mixer and stir for 90 s, subsequently pour the water into the mixer and stir for 240 s. Thirdly, pour the cement mixture into the cylindrical mold with the serrated joint surface mold, then vibrate for 90 s. Fourthly, remove the mold after curing for 24 h. Half jointed cement mortar specimens with various JRCs are shown in Figure 3a. Finally, bond the two-half jointed cement mortar specimens by gypsum after curing for 28 d. The jointed cement mortar specimens after bonding are shown in Figure 3b. Before impact tests, both ends of jointed specimens were polished by a grinding machine to ensure that the non-parallelism at both ends was less than 0.02 mm.

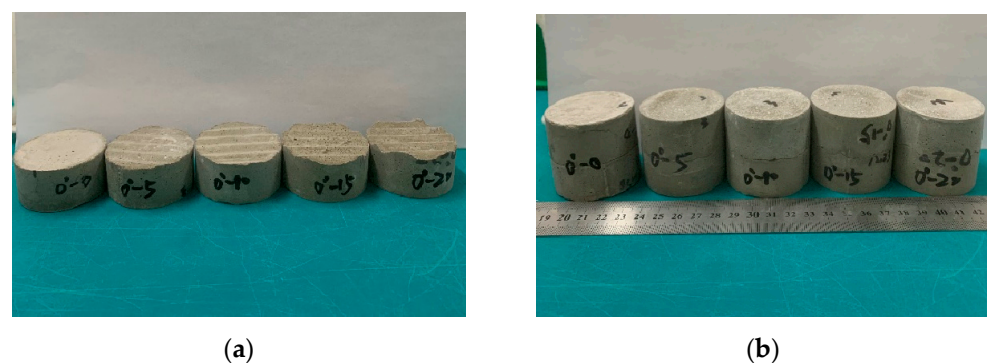


Figure 3. Jointed cement mortar specimen. (a) Half jointed cement mortar specimen, (b) Jointed cement mortar specimen after bonding.

3. Results and Analysis

3.1. Dynamic Stress-Strain Curve Analysis

The dynamic stress-strain curves of jointed specimens with various JRCs and joint inclination angles are illustrated in Figure 4.

As shown in Figure 4, dynamic stress-strain curves show no compaction form but an approximate linear shape in the initial stage. Therefore, the initial stage of the stress-strain curve under impact load is different from that under static load. This phenomenon is more pronounced in complete specimens, whereas jointed specimens exhibit a shorter linear elastic stage. Moreover, the dynamic stress-strain curves of both complete and jointed specimens can be classified into three stages, namely linear elastic, plastic deformation, and post-peak failure.

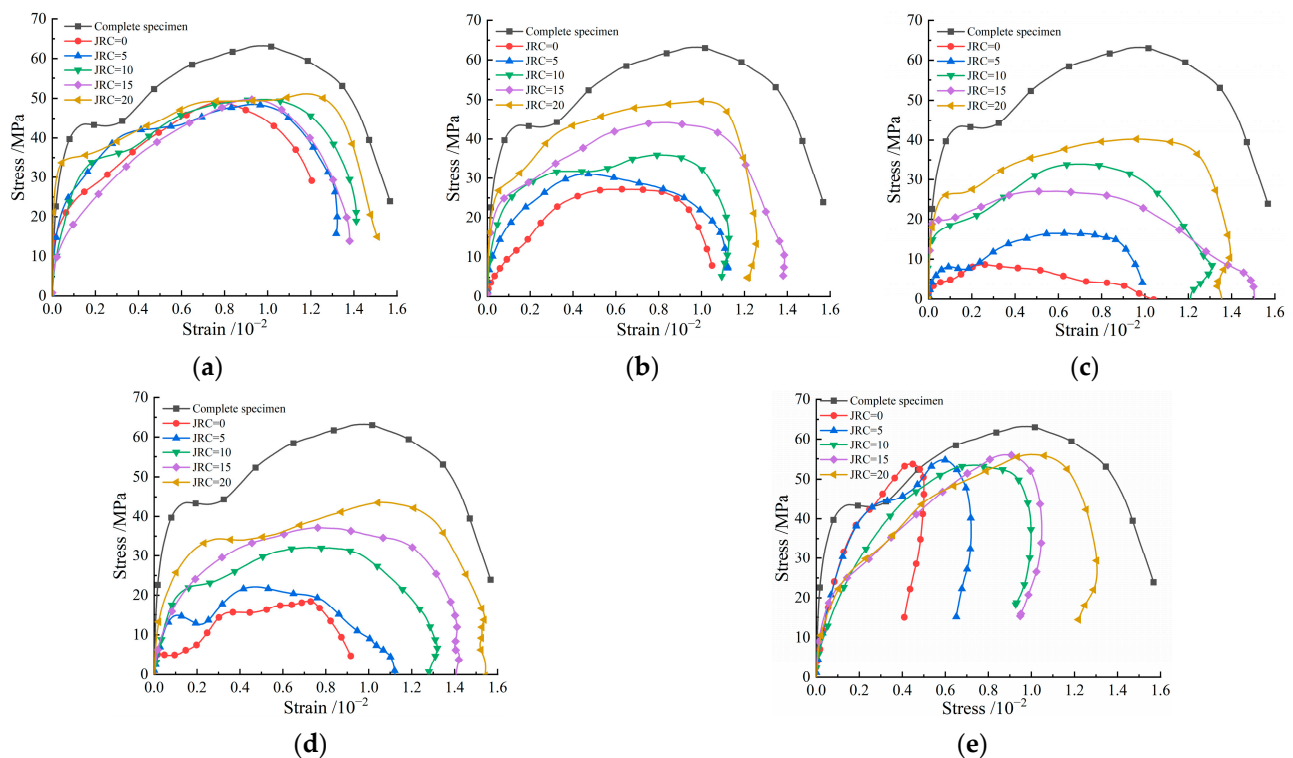


Figure 4. Dynamic stress-strain curves of jointed specimens with various JRCs and joint inclination angles. (a) $\beta = 0^\circ$, (b) $\beta = 30^\circ$, (c) $\beta = 45^\circ$, (d) $\beta = 60^\circ$, (e) $\beta = 90^\circ$.

In the plastic deformation stage, the dynamic stress-strain curves of both complete and jointed specimens exhibit a continuous increase in strain after the first peak, while the stress remains constant. Once the strain reaches a certain level, the stress further increases until the specimen's plastic deformation occurs. At joint inclination angles of 45° to 60° , jointed specimens exhibit a higher susceptibility to sliding failure under impact conditions.

After reaching the peak stress, jointed specimens exhibit softening behavior, characterized by distinct curve profiles with decreasing stress. The post-peak curves of jointed specimens with joint inclination angles of 0° or 90° exhibit an almost linear decline, which indicates pronounced brittle characteristics. Despite being affected by the sliding of the joint surface, jointed specimens with a joint inclination angle of 45° retain a certain load-bearing capacity during the softening stage, as the stress gradually decreases with the strain along the post-peak failure curve.

As illustrated in Figure 4, the dynamic stress-strain curves of jointed specimens are notably influenced by JRC under the same joint inclination angles. When the joint inclination angle is 0° or 90° , jointed specimens with various JRCs exhibit similar curve slopes, peak stresses, and post-peak failure stage slopes, which all indicates pronounced brittleness. When the joint inclination angle is in the range of 30° to 60° , the slope in the initial linear elastic stage of dynamic stress-strain curve progressively augments with JRC increasing, leading to an increase in the elastic modulus. The slope in the plastic deformation stage reveals an increasing resistant capability of deformation with JRC increasing, resulting in a gradual rise in the peak stress. During the post-peak failure stage, when the JRC is 0, jointed

specimens exhibit a notable reduction in slope, indicating plastic failure characteristics. As the JRC increases from 0 to 20, the slope in the post-peak failure stage exhibits a significant increase, indicating a brittle failure.

3.2. Failure Mode of Jointed Specimens with Various JRCs and Joint Inclination Angles

The failure mode of jointed specimens was recorded and analyzed after the impact tests. Figure 5 displays failure photographs of jointed specimens with various joint inclinations when JRC is 0, and Figure 6 presents failure photographs of jointed specimens with various JRCs when the joint inclination angle is 45° .

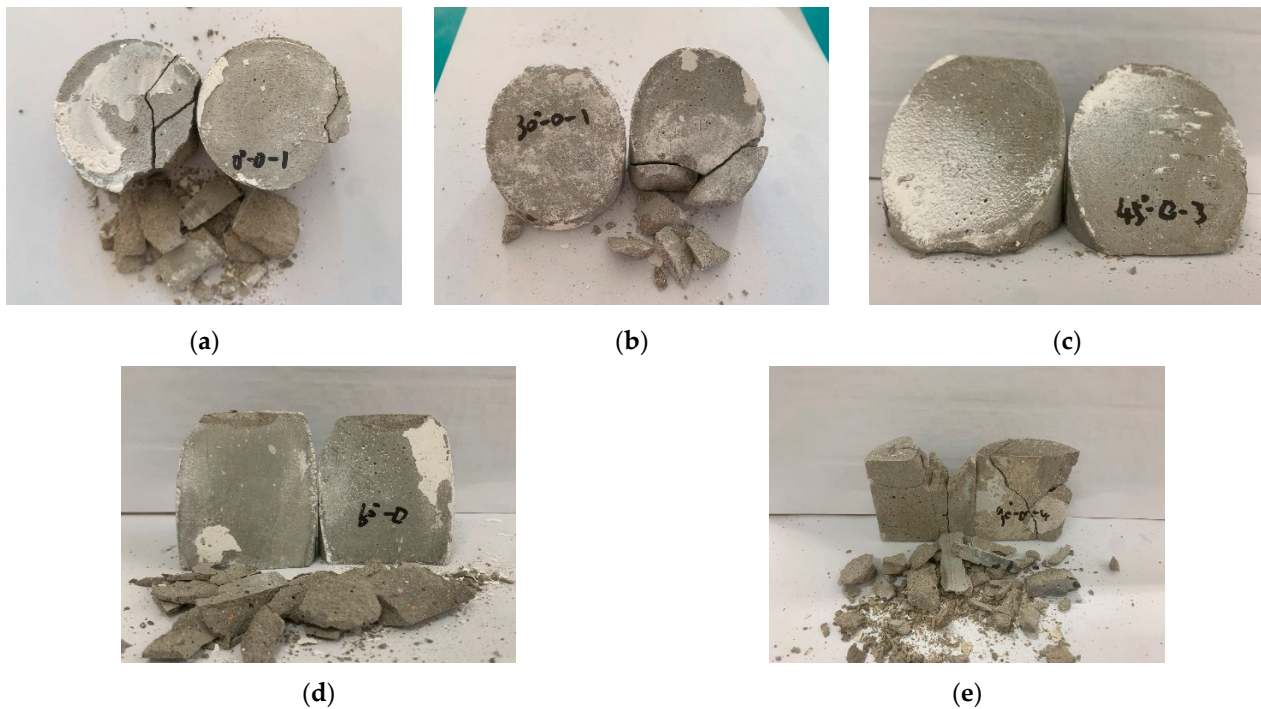


Figure 5. Failure modes of jointed specimens with various joint inclinations when JRC is 0. (a) $\beta = 0^\circ$, (b) $\beta = 30^\circ$, (c) $\beta = 45^\circ$, (d) $\beta = 60^\circ$, (e) $\beta = 90^\circ$.

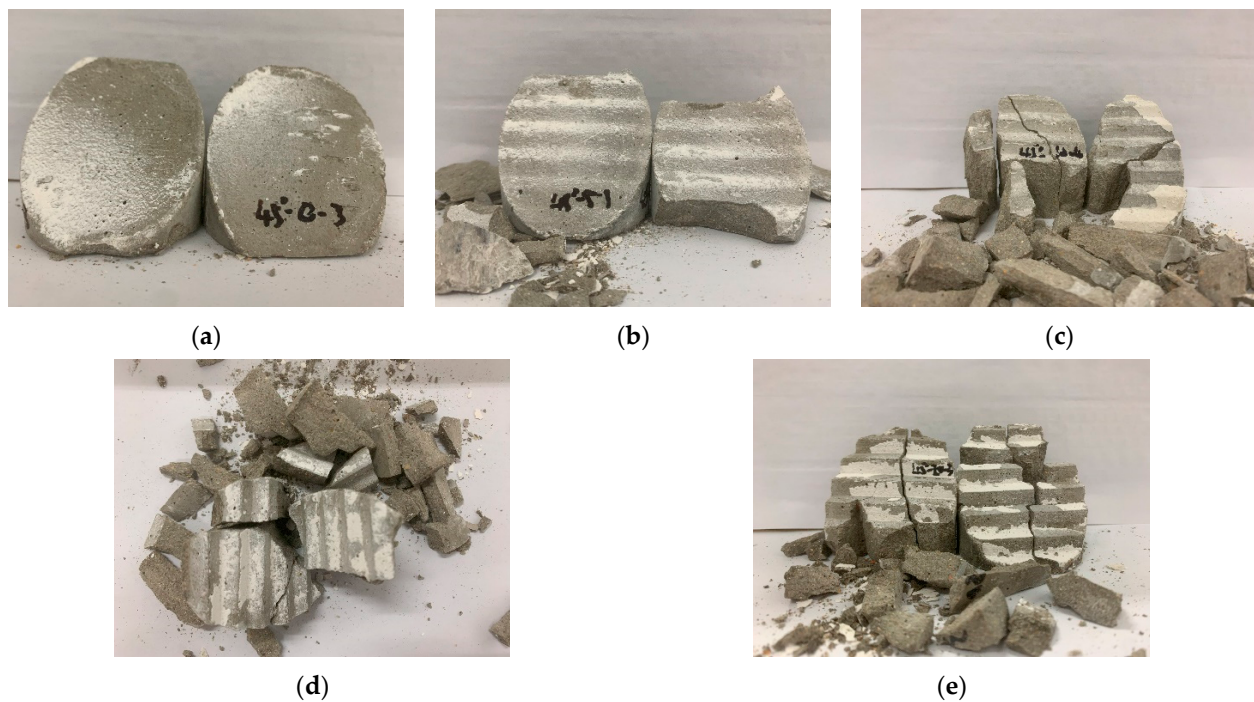


Figure 6. Failure modes of jointed specimens with various JRCs when the joint inclination angle is 45° . (a) JRC = 0, (b) JRC = 5, (c) JRC = 10, (d) JRC = 15, (e) JRC = 20.

The final failure of jointed specimens can be attributed to joint surface slip, shear, or tension, and the failure mode varies with JRC and joint inclination angle. The failure mode of the specimen can be mainly classified into three types.

- (1) Splitting tensile failure parallel to the joint surface. As depicted in Figure 5a,e and Figure 6e, jointed specimens predominantly exhibit splitting tensile failure parallel to the joint surface, resulting in the upper and lower parts of jointed specimens fracturing into multiple uniform-shaped small pieces, along with a few fragments. Regardless of the JRC, the failure of joint specimens with joint inclination angles of 0° or 90° is mainly attributed to splitting tensile, accompanied by a notable lateral expansion phenomenon.
- (2) Shear slip failure along the joint surface. As shown in Figure 5c, the joint surface with JRC of 0 is smooth at this time, hence the shear strength is very low, and the relative dislocation of the joint surface occurs, leading to the shear slip failure. Moreover, the cement mortar on both sides of the slip surface are almost complete, and no penetrating cracks appear.
- (3) Compound failure of splitting tensile and shear. As depicted in Figure 6b–d, when the joint inclination angle decreases or the JRC increases, the failure mode of jointed specimens transfers from shear slip failure to compound failure of splitting tensile and shear. The failure surface partially extends through the cement mortar and partially through the joint surface. Figure 6c,d illustrate that the failure surface involves both cement mortar and joint surface, resulting from the combined failure of tension failure in the cement mortar and shear failure along the joint surface.

3.3. Relationship between Peak Stress, JRC and Joint Inclination

Figure 7 demonstrates the relationship between peak stress, JRC, and joint inclination.

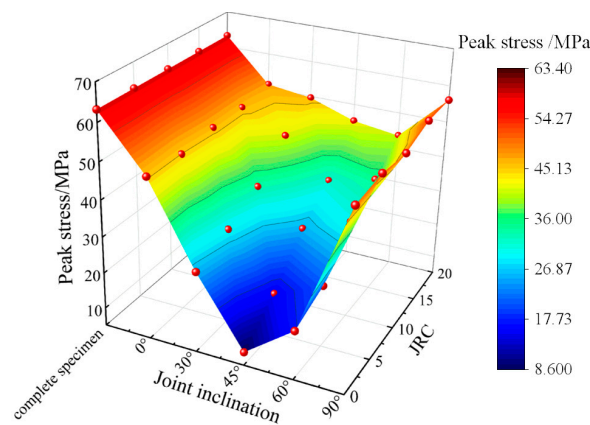


Figure 7. Relationship between peak stress, JRC, and joint inclination angle.

As shown in Figure 7, under similar impact loading, both JRC and joint inclination angle significantly affect the peak stress of the jointed specimens. The peak stress exhibits a trend of initially decreasing and then increasing as the joint inclination angle increases, namely an approximate V-shape variation. On the other hand, the peak stress increases with JRC increasing. For instance, when the JRC is 0, 5, 10, 15, and 20, the average peak stress of jointed specimens with a joint inclination angle of 45° are 8.68 MPa, 16.33 MPa, 27.04 MPa, 33.95 MPa, and 45.26 MPa, respectively. Compared to the complete specimen, the average peak stress has decreased by 86.3%, 74.2%, 57.2%, 46.3%, and 28.4%, respectively. It can be observed that the 90° joint inclination has the least impact on the peak stress, whereas the 45° joint inclination has the greatest effect. With the same JRC, the peak stress tends to decrease nonlinearly with the joint inclination angle ranging from 0° to 45° , while the peak stress demonstrates an overall increasing trend with the joint inclination angle ranging from 45° to 90° . Furthermore, when joint inclination angle is 0° or 90° , the peak stress of jointed specimens is closer to each other regardless of the JRC. This can be attributed to the fact that when the joint surface is parallel or perpendicular to the direction of the loading stress wave, the JRC has a diminished effect on the peak stress, resulting in a weak stress wave reflection.

3.4. Stress Wave Propagation Characteristics of Jointed Specimen

Figure 8 illustrates the stress-time curves of reflected and transmitted waves of jointed specimens with various joint inclination angles subjected to impact load at JRC of 0. The reflection and transmission stress waves exhibit a distinct stepwise variation with time. The transmitted stress waves amplify as the joint inclination angle increases from 0° to 90° . The reflected stress waves display a double peak with the joint inclination angle in the range of 30° to 60° . This can be attributed to the multiple reflections of stress waves within the jointed specimen caused by the presence of serrated joints during stress wave propagation.

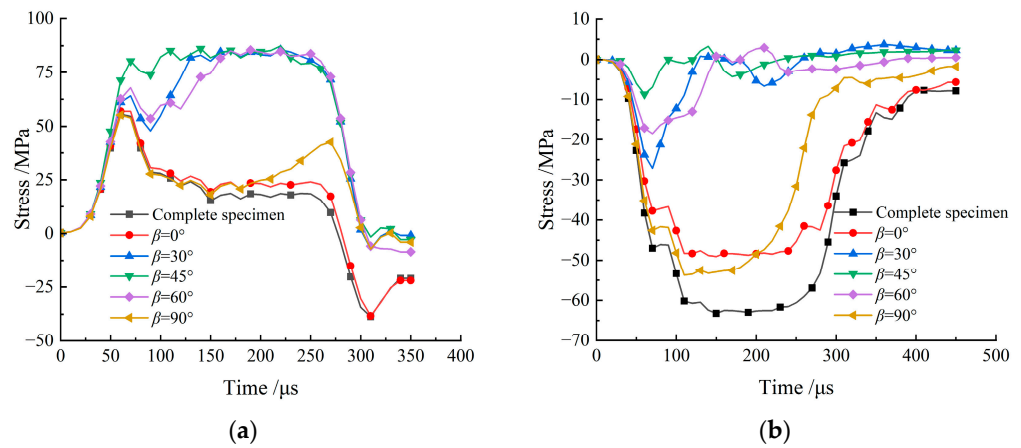


Figure 8. Reflection and transmission stress waves of jointed specimens with various joint inclination angles when JRC is 0. (a) Reflected wave, (b) Transmitted wave.

When JRC is 5, 10, 15, or 20, the propagation characteristics of the stress wave remain consistent with those observed when JRC is 0, which is not further described.

Figure 9 presents the stress-time curves of reflected and transmitted waves of jointed specimens with various JRCs subjected to impact load at joint inclination angle of 60°. It is evident that the difference between the transmitted and reflected stress waves becomes more pronounced. With a constant joint inclination angle, an increase in JRC results in a weak reflected stress wave and a strong transmitted stress wave. This indicates that high JRC leads to a diminished reflection of the stress wave when the joint inclination angle is fixed.

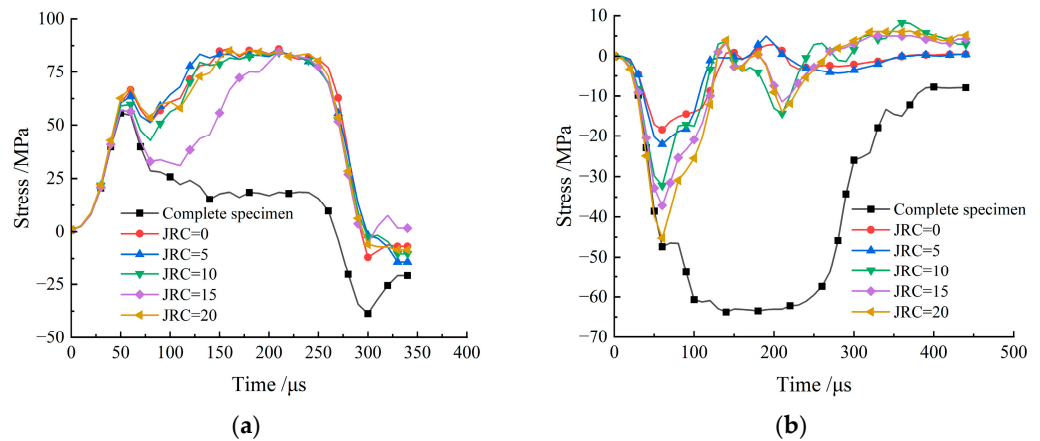


Figure 9. Reflection and transmission stress waves of jointed specimens with various JRCs when the joint inclination angle is 60°. (a) Reflected wave, (b) Transmitted wave.

3.5. Energy Analysis of Jointed Specimen under Impact Load

The energy input of the SHPB apparatus is realized by a bullet impact. According to the assumption of the one-dimensional stress wave theory and ignoring the energy attenuation during the wave propagation in the bar, the incident wave energy E_I , reflected wave energy E_R , and transmitted wave energy E_T can be expressed as:

$$E_I = A_0 C_0 E_0 \int_0^t \epsilon_i^2(t) dt \tag{3}$$

$$E_R = A_0 C_0 E_0 \int_0^t \epsilon_r^2(t) dt \tag{4}$$

$$E_T = A_0 C_0 E_0 \int_0^t \epsilon_t^2(t) dt \tag{5}$$

where E_I , E_R , and E_T representing the energy of incident, reflected, and transmitted waves, respectively; A_0 , C_0 , and E_0 represent the cross-sectional area, longitudinal wave velocity, and elastic modulus of incident and transmission bar.

According to the first law of thermodynamics, the energy during wave propagation should satisfy the following relationship:

$$E_I = E_R + E_D + E_T \tag{6}$$

where E_D represents the energy dissipated by the jointed specimen, which is the irreversible dissipation energy.

In order to reduce the influence of the incident wave energy, reflected energy coefficient and transmitted energy coefficient are introduced to analyze the effect of serrated joints on stress wave propagation quantitatively, and they are calculated as follows:

$$R_r = \frac{E_R}{E_I} \tag{7}$$

$$R_t = \frac{E_T}{E_I} \tag{8}$$

where R_r and R_t represent the reflected energy coefficient and transmitted energy coefficient, respectively.

Figure 10 illustrates the relationship between the average values of the reflected energy coefficient and transmitted energy coefficient with the JRC and joint inclination angle when the stress wave propagates through jointed specimens, as obtained from Table 2. The following patterns can be observed by analyzing Figure 10:

- (1) As the joint inclination angle increases from 0° to 45° , the reflected energy coefficient progressively increases, while the transmitted energy coefficient gradually decreases. On the other hand, with the joint inclination angle increasing from 45° to 90° , the reflected energy coefficient decreases, and the transmitted energy coefficient increases. At the joint inclination angle of 45° , the reflected energy coefficient reaches its maximum value, and the transmitted energy coefficient reaches its minimum value.
- (2) With the increase of JRC from 0 to 20, the reflected energy coefficient gradually increases at joint inclination angles of 0° or 90° , while the transmitted energy coefficient decreases progressively. Additionally, with the increase of JRC, the reflected energy coefficient gradually decreases when joint inclination angle is in the range of 30° to 60° , while the transmitted energy coefficient gradually increases.

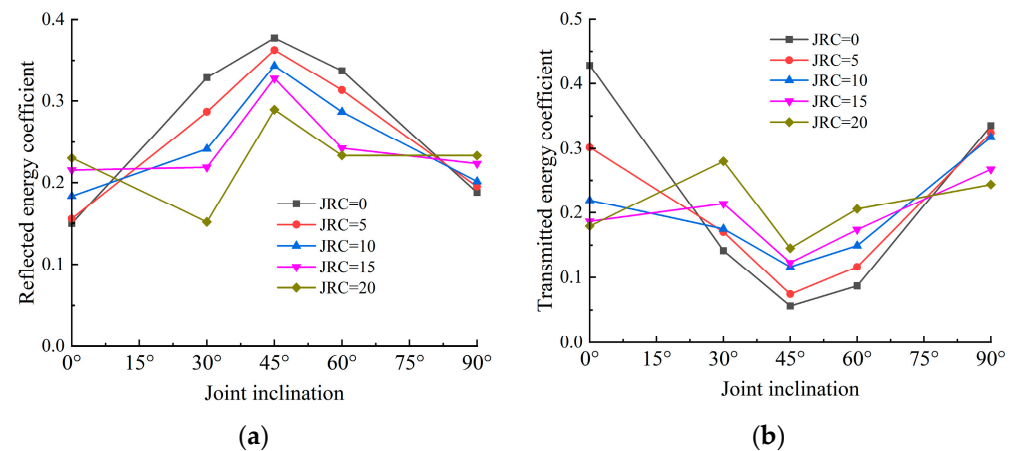


Figure 10. Energy coefficients variation of jointed specimens with various JRCs and angles. (a) Reflected energy coefficient, (b) Transmitted energy coefficient.

Table 2. Energy coefficients of jointed specimens with various JRCs and joint inclination angles.

| Joint Inclination Angle | JRC | Reflected Energy Coefficient | Transmitted Energy Coefficient |
|-------------------------|------|------------------------------|--------------------------------|
| Complete specimen | None | 0.146 | 0.511 |
| 0° | 0 | 0.150 | 0.428 |
| | 5 | 0.155 | 0.302 |
| | 10 | 0.183 | 0.219 |
| | 15 | 0.215 | 0.187 |
| | 20 | 0.230 | 0.179 |
| 30° | 0 | 0.328 | 0.141 |
| | 5 | 0.287 | 0.170 |
| | 10 | 0.241 | 0.175 |
| | 15 | 0.219 | 0.214 |
| | 20 | 0.151 | 0.280 |
| 45° | 0 | 0.377 | 0.067 |
| | 5 | 0.363 | 0.077 |
| | 10 | 0.343 | 0.117 |
| | 15 | 0.328 | 0.123 |
| | 20 | 0.289 | 0.145 |
| 60° | 0 | 0.337 | 0.087 |
| | 5 | 0.313 | 0.118 |
| | 10 | 0.287 | 0.149 |
| | 15 | 0.242 | 0.174 |
| | 20 | 0.233 | 0.205 |
| 90° | 0 | 0.188 | 0.335 |
| | 5 | 0.195 | 0.324 |
| | 10 | 0.201 | 0.317 |
| | 15 | 0.223 | 0.267 |
| | 20 | 0.235 | 0.244 |

4. Discussion

4.1. Discussion on Failure Mode of Jointed Specimen

Underground rock engineering, including tunnels, mining tunnels, and chambers, often encounters jointed rocks. Due to the various combinations of JRC and joint inclination, jointed rocks exhibit anisotropic mechanical properties and failure characteristics. Taking the jointed specimens with various joint inclination angles at JRC of 0 and jointed specimens with various JRCs at joint inclination angle of 45° as examples, the discussion focuses on the failure modes observed.

Figure 5 reveals that at JRC of 0, the jointed specimen with a 0° joint experiences tensile failure parallel to the joint surface, resulting in a fracture surface parallel to the end face. Jointed specimens with 45° or 60° joints exhibit shear failure along the joint surface. In contrast, jointed specimens with a 90° joint primarily undergo splitting tensile failure along the joint surface, accompanied by localized shear failure.

A comparison of failure modes depicted in Figures 5 and 6 reveals that both joint roughness and inclination have obvious effects on the failure modes of jointed rocks. Analyzing the failure modes of jointed specimens in Figure 6, an increase in JRC leads to a notable reduction in fragment size and an increase in their number. At a joint inclination angle of 45°, the presence of a weak structural surface generates shear stress on the joint surface when subjected to load. Cracks initiate from the end of the joint surface and eventually result in shear slip failure. Moreover, as JRC increases, the shear strength of the joint surface increases. At JRC of 5, the jointed specimen is mainly shear failure, accompanied by localized tensile failure at two ends. At JRC of 10 and 15, the damage of jointed specimens intensifies, and cracks propagate downward from the joint surface, causing staggered joint surfaces and destruction at both ends along the axial direction. This

behavior arises due to the combined effects of axial compressive stress and shear stress on the joint surface. At JRC of 20, the integrity of the jointed specimen is improved due to the large height of serrated joints, and cracks generate at the end of the joint surface and propagate along the direction of the joint inclination, exhibiting conspicuous tensile failure. From this point, the jointed specimen experiences only axial splitting failure since the stress cannot reach the shear strength of the joint surface, and the serrated joints remain complete.

In summary, the failure mode of the jointed specimens is strongly influenced by joint roughness and inclination. The presence of joint roughness enhances the shear capacity of the jointed specimens, leading to a gradual transition in the failure mode from shear slip failure to tensile shear failure. However, when the JRC reaches a certain threshold, the stress fails to reach the shear strength of the joint surface, resulting in pure splitting tensile failure. Additionally, an increase in JRC leads to a reduction in fragment size.

4.2. Discussion on Stress Wave Energy Transfer of Jointed Specimen

It is noteworthy that the variation of the reflected energy coefficient and transmitted energy coefficient at the joint inclination angles of 30° to 60° are different from those at 0° and 90° . This phenomenon can be attributed to the following main reasons:

- (1) JRC directly affects the unevenness and contact area. With JRC increasing, the degree of unevenness and contact area increases. At joint inclination angles of 0° or 90° , the uneven joint surface results in a decreased relative contact area, leading to reduced energy transfer. Conversely, at joint inclination angles of 30° to 60° , the uneven joint surface increases the relative contact area, facilitating energy transfer.
- (2) The unevenness of joint surface results in the scattering and reflection of incident waves. At joint inclination angles of 0° or 90° , scattering and reflection significantly impede wave propagation and reduce the transmission energy coefficient. Moreover, at joint inclination angles of 30° to 60° , the hindrance to wave propagation is less pronounced, thereby increasing the transmission energy coefficient.
- (3) The propagation paths of stress waves in jointed rocks vary with the joint inclination. At joint inclination angles of 0° or 90° , stress waves propagate perpendicular to or parallel to the joint surface. Hence, increasing JRC enhances the scattering and reflection of stress waves, reducing stress wave transmission. Conversely, at joint inclination angles of 30° to 60° , the wave propagation path becomes relatively oblique. The increased JRC weakens the scattering and reflection of incident waves, thereby increasing stress wave transmission.

The influence of joint roughness and inclination on stress wave propagation in jointed rocks is highly complex. Additionally, the effects of joints on stress wave propagation vary with joint morphologies and inclinations. The roughness of different parts of the joint surface is not uniform, and joint rock surface failure can involve one or multiple failure modes at various joint inclinations. For instance, for 0° or 90° joints, jointed rocks primarily exhibit splitting tensile failure as the dominant failure mode, with minimal sensitivity to joint roughness. However, for a 45° joint, shear failure is observed in jointed rocks with low roughness, while high roughness leads to tensile shear failure. The investigated joint surface roughness and inclination angle in this study represent only one specific scenario of jointed rocks. Further research is required to explore various joint morphologies and inclination angles.

5. Conclusions

The effects of joint roughness and inclination on the dynamic mechanical properties, stress wave propagation characteristics, and failure mode of jointed rocks have been investigated by conducting impact tests for prefabricated serrated joint cement mortar specimens. The conclusions are drawn as follows.

- (1) Both joint roughness and inclination have certain effects on the peak stress of the jointed specimen. The peak stress initially decreases then increases with the increase of the joint inclination angle, namely a V-shape variation. The influence of JRC on the

peak stress of jointed specimens is negligible at inclination angles of 0° or 90° . The peak stress gradually increases with JRC increasing when the joint inclination angle is in the range of 30° to 60° . Jointed specimens exhibit the lowest peak stress at an inclination angle of 45° and JRC of 0.

- (2) The existence of joint inclination and roughness affect the stress wave propagation through the jointed specimen. When the JRC increases from 0 to 20, the reflection of stress waves on the joints gradually increases, and the transmission decreases for the joint inclination angles of 0° and 90° . On the contrary, when the joint inclination angle is in the range of 30° to 60° , the reflection of stress waves on the joints gradually decreases, and the transmission gradually increases with JRC increasing from 0 to 20.
- (3) The effect of JRC on the failure mode under impact load is significant. Jointed rocks exhibit three typical failure modes, namely splitting tensile failure parallel to the joint surface, shear slip failure along the joint surface, and compound failure of splitting tensile and shear.
- (4) Joint roughness and inclination influence the energy transfer through jointed rocks. With the joint inclination angle increasing, reflected energy coefficient initially increases then decreases, while the transmitted energy coefficient initially decreases then increases. At joint inclination angles of 0° or 90° , the reflected energy coefficient increases with the increase of JRC from 0 to 20, while the transmitted energy decreases. However, when joint inclination angles are in the range of 30° to 60° , the reflected energy coefficient gradually decreases with JRC increasing, while the transmitted energy coefficient gradually increases.

Author Contributions: Conceptualization, P.Y.; Software, Q.Z.; Validation, A.L.; Formal analysis, A.L.; Data curation, C.C.; Writing—original draft, A.L.; Writing—review & editing, P.Y. All authors have read and agreed to the published version of the manuscript.

Funding: This work was funded by Anhui Provincial Natural Science Foundation (No. 2108085ME156 and No. 1808085QE148), China Postdoctoral Science Foundation (No. 2018M642504), The University Synergy Innovation Program of Anhui Province (No. GXXT-2022-020), and Natural Science Research Project of Colleges and Universities in Anhui Province (No. KJ2017A097).

Data Availability Statement: The data used to support the findings of this study are available from the corresponding author upon request.

Conflicts of Interest: The authors declare no conflict of interest.

References

1. Xie, H.P. Research framework and anticipated results of deep rock mechanics and mining theory. *Eng. Sci. Technol.* **2017**, *49*, 1–16. [[CrossRef](#)]
2. Xie, H.P.; Gao, F.; Ju, Y.; Gao, M.Z.; Zhang, R.; Gao, Y.N.; Liu, J.F.; Xie, L.Z. Quantitative definition and investigation of deep mining. *J. China Coal Soc.* **2015**, *40*, 1–10. [[CrossRef](#)]
3. Su, H.J.; Guo, Q.Z.; Jing, H.W.; Hu, C.G. Mechanical properties of rock mass with built-in rough joints based on 3D printing. *J. Min. Saf. Eng.* **2021**, *38*, 840–846. [[CrossRef](#)]
4. Zhu, W.S.; Zhou, K.; Yu, D.J.; Wang, L.G.; Ma, Q.S. Damage mechanics analysis and field monitoring of brittle fractured surrounding rock. *J. Rock Mech. Eng.* **2010**, *29*, 1963–1969.
5. Li, N.N.; Li, J.J.; Li, H.B.; Liu, T.T.; Chai, S.B. SHPB experiment on influence of contact area of joints on propagation of stress wave. *J. Rock Mech. Eng.* **2015**, *34*, 1994–2000. [[CrossRef](#)]
6. Li, Y.X.; Wang, Y.Y.; Cao, L.T. Effects of rough jointed rock mass using 3D printing technology on stress wave energy propagation. *Exp. Mech.* **2023**, *38*, 267–275.
7. Wang, L.M.; Zhao, J.; Hua, A.Z.; Song, H.W. The Progress in Study of Regularity of a Stress Wave Propagation in the Jointed Rock Mass. *Rock Soil Mech.* **2003**, 602–605+610. [[CrossRef](#)]
8. Pyrak-Nolte, L.J. The seismic response of fractures and the interrelations among fracture properties. *Int. J. Rock Mech. Min. Sci. Geomech. Abstr.* **1996**, *33*, 787–802. [[CrossRef](#)]
9. Cai, J.G.; Zhao, J. Effects of multiple parallel fractures on apparent attenuation of stress waves in rock masses. *International J. Rock Mech. Min. Sci.* **2000**, *37*, 661–682. [[CrossRef](#)]
10. Zhou, Z.; Zhang, L.; Hou, H. Study on impact from filling on mechanical properties and energy evolution of jointed rock mass. *Water Resour. Hydropower Eng.* **2020**, *51*, 117–123. [[CrossRef](#)]
11. Liu, M.; Liu, E. Dynamic mechanical properties of artificial jointed rock samples subjected to cyclic triaxial loading. *Int. J. Rock Mech. Min. Sci.* **2017**, *98*, 54–66. [[CrossRef](#)]
12. Wang, P.T.; Huang, Z.Z.; Ren, F.H.; Zhang, L.; Cai, M.F. Research on direct shear behaviour and fracture patterns of 3D-printed complex jointed rock models. *Rock Soil Mech.* **2020**, *41*, 46–56. [[CrossRef](#)]
13. Li, D.; Liu, M.; Han, Z.; Zhou, Z. Dynamic compressive mechanical properties of bedding sandstone with pre-existing hole. *J. China Coal Soc.* **2019**, *44*, 1349–1358. [[CrossRef](#)]
14. Li, D.Y.; Wong, L.N.Y.; Liu, G.; Zhang, X.P. Influence of water content and anisotropy on the strength and deformability of low porosity sedimentary rocks under triaxial compression. *Eng. Geol.* **2012**, *126*, 46–66. [[CrossRef](#)]
15. Qiu, J.; Li, D.; Li, X.; Zhou, Z. Dynamic fracturing behavior of layered rock with different inclination angles in SHPB Tests. *Shock Vib.* **2017**, *2017*. [[CrossRef](#)]
16. Indraratna, B.; Jayanathan, M.; Brown, T. Shear Strength Model for Overconsolidated Clay-Infilled Idealised Rock Joints. *Fac. Eng. Pap.* **2008**, *58*, 55–65. [[CrossRef](#)]
17. Indraratna, B.; Oliveira, D.A.F.; Brown, E.T.; de Assis, A.P. Effect of Soil-Infilled Joints on the Stability of Rock Wedges Formed in a Tunnel Roof. *Int. J. Rock Mech. Min. Sci.* **2010**, *47*, 739–751. [[CrossRef](#)]
18. Walton, G.; Alejano, L.R.; Arzua, J.; Markley, T. Crack damage parameters and dilatancy of artificially jointed granite samples under triaxial compression. *Rock Mech. Rock Eng.* **2018**, *51*, 1637–1656. [[CrossRef](#)]
19. Crampin, S. A Review of wave motion in anisotropic and cracked elastic-media. *Wave Motion* **1981**, *3*, 343–391. [[CrossRef](#)]
20. Hudson, J.A. Wave speeds and attenuation of elastic waves in material containing cracks. *Geophys. J. Int.* **1981**, *64*, 133–150. [[CrossRef](#)]
21. Dai, F.; Huang, S.; Xia, K.; Tan, Z. Some fundamental issues in dynamic compression and tension tests of rocks using split hopkinson pressure bar. *Rock Mech. Rock Eng.* **2010**, *43*, 657–666. [[CrossRef](#)]
22. Kahraman, S. The Effects of fracture roughness on p-wave velocity. *Eng. Geol.* **2002**, *63*, 347–350. [[CrossRef](#)]
23. Liu, H.Y.; Deng, Z.D.; Wang, X.S.; Zhang, J.H.; Zhang, L.M. Similar material test study of dynamic failure of jointed rock mass with SHPB. *Rock Soil Mech.* **2014**, *35*, 659–665. [[CrossRef](#)]
24. Ju, Y.; Li, Y.X.; Xie, H.P.; Song, Z.Z.; Tian, L.L. Stress wave propagation and energy dissipation in jointed rocks. *Chin. J. Rock Mech. Eng.* **2006**, *25*, 26–34.
25. Li, Y.X.; Liu, J.F.; Qin, L. Experimental study on rule of energy dissipation of stress wave across rock joint. *J. Exp. Mech.* **2011**, *26*, 85–90.
26. Li, Y.X.; Xie, H.P.; Zhu, Z.M.; Feng, H.D.; Ye, J.J. Study on rules of transmission and reflection of stress wave across fractal joint. *Chin. J. Rock Mech. Eng.* **2009**, *28*, 120–129.
27. Li, X.L.; Wang, J.G.; Zhang, Z.Y.; Huang, Y.H. Experimental study for effects of strain rates and joint angles on dynamic responses of simulated rock materials. *Explos. Shock Waves* **2016**, *36*, 483–490.
28. Yang, Y.; Yang, R.S.; Wang, J.G. Simulation material experiment on dynamic mechanical properties of jointed rock affected by joint thickness. *J. China Univ. Min. Technol.* **2016**, *45*, 211–216+309. [[CrossRef](#)]
29. Zhang, W.; Zhou, G.Q.; Zhang, H.B.; Zhang, Y. Experimental research on the influence of obliquity on the mechanical characteristics of a fractured rock mass. *J. China Univ. Min. Technol.* **2009**, *38*, 30–33.
30. Ping, Q.; Wang, S.; Wu, Y.Y.; Sun, S.J.; Shen, K.; Wang, C.; Gao, Q.; Fang, C. Study on mechanical properties and energy consumption of fissured sandstone with different dip angles under impact load. *Shock Vib.* **2022**, *2022*, 1–9. [[CrossRef](#)]

31. Wang, J.G.; Gao, Q.C.; Lu, H.; Liang, S.F.; Huang, B.; Yang, Z. Impact response tests of layered medium with SHPB. *Vib. Shock* **2015**, *34*, 192–197. [[CrossRef](#)]
32. Wang, J.G.; Liang, S.F.; Gao, Q.H.; Li, X.L.; Wang, L.N.; Zhao, Y. Experimental study of jointed angles impact on energy transfer characteristics of simulated rock material. *J. Cent. South Univ. (Sci. Technol.)* **2018**, *49*, 1237–1243.
33. Zou, F.; Li, H.B.; Zhou, Q.C.; Mo, Z.Z.; Zhu, X.M.; Niu, L.; Yang, F.W. Experimental study of influence of joint space and joint angle on rock fragmentation by TBM disc cutter. *Rock Soil Mech.* **2012**, *33*, 1640–1646. [[CrossRef](#)]
34. Chen, X.; Wang, S.Z.; Li, L. Characteristics of fragments of jointed rock mass model under uniaxial compression. *Chin. J. Rock Mech. Eng.* **2012**, *31*, 898–907.
35. Li, S.Z.; Wang, L.; Li, S.C.; Han, J.X. Post-peak deformation and failure experimental study of rock-like specimens with different inclination angles persistent joints. *Chin. J. Rock Mech. Eng.* **2013**, *32*, 3391–3395.
36. Tsubota, Y.; Iwakoke, Y.; Yoshinaka, R.; Yamaguchi, K. Dynamic mechanical properties of rock joints under cyclic loading using ryoke gneiss. In Proceedings of the ISRM International Symposium—8th Asian Rock Mechanics Symposium, Sapporo, Japan, 14–16 October 2014.
37. Xie, H.P. Fractal description of rock joints. *Chin. J. Geotech. Eng.* **1995**, *17*, 18–23.

Disclaimer/Publisher’s Note: The statements, opinions and data contained in all publications are solely those of the individual author(s) and contributor(s) and not of MDPI and/or the editor(s). MDPI and/or the editor(s) disclaim responsibility for any injury to people or property resulting from any ideas, methods, instructions or products referred to in the content.